# Modeled and observed fast flow in the Greenland ice sheet

Ed Bueler

Dept. Mathematics and Statistics, University of Alaska, Fairbanks, Alaska, USA

Constantine Khroulev

Geophysical Institute, Fairbanks, Alaska, USA

Andreas Aschwanden

Arctic Region Supercomputing Center, Fairbanks, Alaska, USA

Ian Joughin

Polar Science Center, Applied Physics Lab, University of Washington, Seattle, Washington, USA

Ben E. Smith

Polar Science Center, Applied Physics Lab, University of Washington, Seattle, Washington, USA

Satellite surface velocity measurements covering 86% of the Greenland Ice Sheet were used to evaluate a prognostic ice dynamics model on a 3 km grid. A small, but systematic, exploration of the parameter space considered changes in just three critical model parameters, describing ice softness, nonlinear basal rheology, and basal water pressure, respectively. Parameter combinations were evaluated by comparing the modeled and observed surface speeds. Best fit to the observed distribution of fast flow occurred with no enhancement of ice softness, nearly-plastic basal material, and high basal water pressure under fast-flowing ice. The use of a standard amount of ice flow enhancement was seen to generate a distribution of fast flow which is fundamentally different from that in the observed flow, while a specific parameterization of basal sliding generated a close-to-observed distribution.

## 1. Introduction

Recent studies have led to a better understanding of the present condition of the Greenland ice sheet (GrIS). Improved surface temperature [*Fausto et al.*, 2009] and precipitation [*Burgess et al.*, submitted] maps are available, for example, as are the horizontal surface velocities for a majority of the GrIS area [*Joughin et al.*, submitted].

In terms of the response of the ice flow to possible climate changes, however, critical quantities like ice softness and basal material strength remain poorly-constrained on a whole-sheet scale. Ice flow models are therefore needed to understand even the present flow state of the GrIS. If reliable predictions for future behavior are to be made, modelers must connect relatively-rich present-day surface observations to a carefully-chosen set of parameters controlling the modeled three-dimensional ice fluid and its basal sliding.

A primary connection is the "inversion" of surface velocities to compute basal stress. Typically hundreds to millions of adjustable spatially-distributed basal parameters are set in such procedures [e.g. *Joughin et al.*, 2004]. Though such inverse modeling is vital to understanding ice flow physics, and potentially so to forecasting ice sheet behavior, it raises the concern of *model error*, which is to say the error from fitting an inappropriate model to the data. Inversion procedures might use ice temperatures from a time-dependent model to determine ice softness, for example, but model error occurs if the inversion yields a description of ice flow which is greatly-different from that which determined the temperature field. Inversion may be used for the initialization of the future runs of prognostic models, but the avoidance of model error requires evidence that the prognostic model can do a reasonable job without inversion.

For these reasons, we asked in this study how a model can match the observed surface velocities using just *three* scalar parameters. Our goal was to explain, by example, what kind of prognostic model might best supply ice temperature and basal melt rate to an inversion of surface velocities, or supply velocity boundary conditions to a regional ice flow model. We used a physically-based formulation of ice flow and basal sliding, and we imposed the present-day climate. We created a small set of century-length model runs on a 3 km grid, and we evaluated the (transient) final state of each model run by comparing its surface velocity to newly-assembled surface velocity measurements.

## 2. Model

The open source Parallel Ice Sheet Model (PISM) has a unified treatment of stresses, sliding resistance, and thermodynamics, with the same physics applied at all points of the ice sheet. It uses a new hybrid membrane- and shear-stress balance scheme for ice flow [*Bueler and Brown*, 2009]. Additionally, for GrIS the runs here, a new conservation of energy scheme determined the ice temperature in cold ice, the liquid water fraction in temperate ice, and the basal melt rate, all from a single enthalpy field [*Aschwanden and Blatter*, 2009].

The basal material of the GrIS is actually a spatially-heterogeneous combination of liquid water, deforming wet- and/or-dirty ice, deforming till, and cold-or-temperate ice sliding over, or frozen to, bedrock. The spatial distribution of these cases is not known in detail for the whole GrIS. All of these conditions were modeled by one basal-sliding power law. This power law permits many interpretations, including classical sliding [*Weertman*, 1964] and till deformation [*Clarke*, 2005]. We choose to describe our basal deformation model as a partially-saturated, nearly-plastic till with


0094-8276/09/$5.00

drainage [compare *Tulaczyk et al.*, 2000]. The unsaturated till strength (friction angle) is a time-independent function of bed elevation, according to the hypothesis that basal material with a marine history should be weak [*Huybrechts and de Wolde*, 1999].

When an ice sheet is sliding, or when a thin basal layer of ice or till is deforming easily, the rate of horizontal motion of the ice column above is controlled significantly by "pushing" and "pulling" on its ice column neighbors. Therefore our flow model included membrane stresses in a balance called the shallow shelf approximation (SSA; [*MacAyeal*, 1989; *Weis et al.*, 1999]). We used a form of this model applicable to entire ice sheets [*Schoof*, 2006], and not just to individual ice streams. Both the classical shallow ice approximation with no sliding (SIA; [*Hutter*, 1983]) and the SSA are solved everywhere at every time step. The solution of the latter always said "zero sliding" for the majority of the ice sheet base, however, because the till was sufficiently strong (e.g. it is frozen) and/or the driving stress was too low. The region of sliding evolved as the geometry and basal melt rate fields evolved. The combined model used the SSA as a "sliding-law" for the SIA [*Bueler and Brown*, 2009].

Our application of PISM to the GrIS used a $501 \times 935$ horizontal grid with 3 km spacing, and a vertical grid with 5 m spacing close to the ice base. Each of the 100 model year runs below used only 5 wall-clock hours (600 processor-hours) of computation time, which suggests that our model can be applied for extensive, fine grid century- and millenial-scale climate scenario studies using supercomputers.

## 3. Observations and model inputs

The observed velocities were an average of four winter velocity maps (2000,2006–2008) derived from RADARSAT data [*Joughin et al.*, submitted], with the (temporal) average weighted by the formal errors for each individual estimate. In a few areas where large changes occurred from 2000 to 2008, the resulting estimate represented some intermediate value. The individual maps were derived from a combination of speckle tracking and conventional interferometry synthetic aperture radar (InSAR) [*Joughin*, 2002]. The mean measurement and processing errors in each velocity component were less than 2 m/yr in areas of low surface slope, with an additional slope-dependent error of 3%. Therefore, especially for fast flowing ice, observational errors were substantially smaller than the model-versus-observed velocity differences below.

Ice surface elevation, land elevation in ice-free areas, and bedrock elevation were from *Bamber et al.* [2001]. Bathymetry from *Jakobsson et al.* [2008] was combined with the bedrock and ice-free land elevation to create a continuous bed elevation map for the entire model domain. The result had limited resolution for subglacial fjord-like topography, with currently-unavoidable consequences for modeling fast-flowing ice in outlet glaciers.

The *Shapiro and Ritzwoller* [2004] data set for geothermal flux was used as a boundary condition at the base of the ice. This smoothly-varying map lacked small-scale features, so our results were not consequences of geothermal spatial variations.

We hypothesized a steady climate for both the "spin-up" preparatory stage and for our parameter study runs. The *Fausto et al.* [2009] parameterization of present, near-surface (2 m) air temperature provided the upper boundary condition for the conservation of energy model. A positive degree day melt model determined upper surface mass balance from precipitation [*Burgess et al.*, submitted] and air temperature. The base of floating ice melted at a uniform heat flux of $0.5\ \mathrm{W\,m^{-2}}$. Ice shelves (floating tongues) calved-off at the location of the present-day calving front.

## 4. Parameter study

As noted, the model runs only differed by the values of three primary parameters. We now describe their roles in the model.

The Glen flow law for ice [*Paterson*, 1994] relates the strain rate tensor $D$ to the deviatoric stress tensor $\tau$,

$$D = e\,A|\tau|^{n-1}\tau. \tag{1}$$

Here $A$ is a fixed scalar function of ice temperature and liquid water fraction [*Lliboutry and Duval*, 1985; *Paterson and Budd*, 1982], $|\tau|$ is a norm (scalar invariant) of the stress tensor $\tau$, and $n = 3$. The scalar *enhancement factor* $e$ was one of our primary parameters, taking values $e = 1, 3, 5$ in the study. Larger values of $e$ imply higher strain rates for the same stress state, thus softer ice, while $e = 1$ is no enhancement.

The shear stress $\tau_b$ applied to the base of the ice sheet was proportional to a power of the sliding velocity:

$$\vec{\tau}_b = -\tau_c \frac{\vec{u}_b}{|\vec{u}_b|^{(1-q)} u_0^q}. \tag{2}$$

The perfectly-plastic case has $q = 0$, implying that the shear stress is independent of the velocity magnitude [*Schoof*, 2006]. The scalar coefficient $\tau_c$ is here called the "yield stress" for any value of $q$, though this interpretation is literal only when $q = 0$ [*Clarke*, 2005]. The *pseudo-plasticity exponent* $0 \le q \le 1$ was one of our primary parameters, taking values $q = 0.10, 0.25, 0.50$. Smaller $q$ values meant more-plastic till. We fixed $u_0 = 100\,\mathrm{m\,a^{-1}}$, interpretable as a "threshold speed". Equation (2) includes the linear till case by using $q = 1$, so that $\tau_b = -\beta u_b$ where $\beta = \tau_c/u_0$ [compare *MacAyeal*, 1989]. *Weertman* [1964]-type obstacle-controlled sliding has $|\vec{u}_b| = C|\vec{\tau}_b|^{(m+1)/2}$, with correspondence $q = 2/(m+1)$ (for appropriate $C$), so equation (2) includes the case of ice sliding over hard bedrock.

The basal material (till) is partially-saturated. The key connection of saturation to strength (yield stress) is through the modeled liquid water pressure within the till, the pore water pressure $p_w$. We used a simplified, local parameterization [*Bueler and Brown*, 2009] which gives $p_w$ as a fraction of the overburden pressure:

$$p_w = \alpha\, w \rho g H \qquad \text{in} \qquad \tau_c = (\tan\phi)(\rho g H - p_w). \tag{3}$$

Here $H$ is the ice thickness, $\rho g H$ is the overburden pressure, and the till fraction angle $\phi$ is discussed below. The relative amount of stored water in the till, a fraction $0 \le w \le 1$, came from time-integrating the basal melt rate at each basal location independently. Excess water drained when the thickness of stored water reached 2 m (the limit $w = 1$). Frozen till has $w = 0$ so that $p_w$ is zero and $\tau_c$ is large. The coefficient $\alpha$ is the *allowed pore water pressure fraction*, the third of our primary parameters, taking values $\alpha = 0.95, 0.98, 0.99$. Observations of boreholes drilled through temperate ice to bedrock support our assumption that $\alpha \approx 1$ [*Lüthi et al.*, 2002] in fast flow regions, while in regions of cold base $w = 0$ occurs, so the constant value of $\alpha$ is inactive.

The yield stress $\tau_c$ in equation (3) is also a function of a spatially-distributed material strength factor $\tan\phi$. The till friction angle $\phi$ in our GrIS model was between 5 and 20 degrees [compare table 8.1 in *Paterson*, 1994]. It was a continuous function of bed elevation, with $\phi = 5$ for bed

elevations lower than 300 m below sea level, $\phi = 20$ for beds higher than 700 m above sea level, and linearly-increasing between.

Of the nine runs in our parameter study, the first was a control run with $(e, q, \alpha) = (3, 0.25, 0.98)$, supposed to be mid-range values. From the control run we created six variations by shifting one primary parameter up or down: $e = 1$, $e = 5$, $q = 0.10$, $q = 0.50$, $\alpha = 0.95$, $\alpha = 0.99$. We added a no-enhancement ($e = 1$), no-sliding, SIA-only run, in which parameters $q$ and $\alpha$ were inactive. (Later we added a final case, called "best run" and explained below.)

Each model run used the same present-day steady climate and initial geometry. The initial enthalpy field was generated by fixing the control run parameters for a 120,000 model year equilibriation run on a 10 km grid with fixed, present-day geometry and climate. For each parameter combination, the model was run for two consecutive 100 model year periods on a 5 km grid, with evolving upper surface. The present geometry was reset after each of these runs, so that the enthalpy field evolved to be more compatible both with the parameter choices and with the present geometry. The model was then run, starting again from present geometry, on the 3 km grid for 100 model years. The transient (modeled) surface velocity field from the end of the run was compared to the observed surface velocity map, with the following results.

## 5. Results

Figure 1 shows the observed surface speed alongside two model results. All nine model results showed slow flow in the interior of the ice sheet, and fast outlet glacier (or ice stream) flow in roughly the right locations. More precise methods than such "eyeballing" are needed for evaluating model results, however, so we computed the average absolute and root-mean-square (RMS) differences between modeled and observed surface speeds. By these standards, the $e = 1$ runs, both with and without sliding, are the best results, showing 19 m/a average and 50 m/a RMS differences in both cases. For comparison, the worst result was for the $e = 5$ run, with 46 m/a average and 71 m/a RMS differences.

On the other hand, such a direct comparison of surface speeds over the observed portion of the GrIS area requires cautious interpretation. Fast flow features of the GrIS make up a small areal fraction, but changes to the flow in these regions would be the most significant in its response to climate changes. While the model may mis-locate these fast flow features, because of a lack of spatially-detailed basal strength and bed topography as inputs, it is still appropriate to ask a model to produce surface speed *distributions* of the right type. Close model approximation to the observed fast flow distribution suggests credible modeled ice volume evolution over century- and millenial-time-scales.

Figure 2 compares the observed fast flow distribution to the modeled results from three runs. Note that observed surface speeds in excess of 100 m/a occur in 8.5% of the GrIS area. Observed speed above 3000 m/a occur in only 45 of the $2 \times 10^5$ ice-filled cells of the 3 km grid, however, so we exclude these cells as being too few to support meaningful comparison with model results. Thus Figure 2 shows the histogram of surface speeds in each of 30 bins of width 100 m/a, from 0 m/a to 3000 m/a. The vertical scale is logarithmic, emphasizing differences in the amount of fast flow. The left-most bin contain those 91.5% of grid cells with observed speeds in the 0–100 m/a range, and the previous average and RMS differences essentially evaluate this 91.5%.

By this comparison scheme, the SIA-only run without sliding performs poorly (Figure 2). It has far too few grid cells with speeds above 500 m/a. The $e = 1$ run with sliding performs only slightly better because the control run values of $q$ and $\alpha$ do not yet generate adequate sliding (not shown). All of the enhanced ($e = 3, 5$) runs in the parameter study give better distributions of fast flow than the SIA-only and $e = 1$ runs, at least for speeds $\gg 100$ m/a (not shown). However, in each such enhanced case we note an excessive amount of flow in the 100–300 m/a range, compared to observations. For an example illustrating this effect, the green "+" in the second-from-left bin in Figure 2, shows that the control run has 2.2 times as many cells with speeds in 100–200 m/a range as are observed.

The results of the original cases of the parameter study showed that using the most-plastic till ($q = 0.10$) and the highest-allowed pore water pressure ($\alpha = 0.99$) gave better fast flow distributions. Therefore we added a run with $(e, q, \alpha) = (1, 0.10, 0.99)$. This un-enhanced "best run" was indeed best in its fast flow distribution (Figure 2). Also it had only 0.17% fewer cells with speeds in the 100–200 m/a range than were observed. Finally this run produced 23 m/a average and 56 m/a RMS differences, close to the best in the study (above). Map-plane Figure 1 shows that the "best run" reproduced several features of the observed speed map, including a well-delineated NE Greenland ice stream and an appropriately-wide region of very slow flow near the divide.

## 6. Discussion and Conclusion

An ice-softening enhancement factor has been included in most ice sheet models of the GrIS [e.g. *Huybrechts and de Wolde*, 1999] because it increases the ice flow speed, bringing the ice sheet volume closer to observed values for long model-time runs. Though we believe this to be the primary actual justification for enhancement, it must also be justified in part by the presence of dusty and/or anisotropic, thus softer, ice. The effect of adding enhancement, however, is clear in our results: if $e = 3$ or $e = 5$ then there is too much surface speed in the 100–300 m/a range. Many model studies may have mis-ascribed the surface expression of basal sliding, or of the deformation of soft, dirty temperate ice in thin basal layers, to these bulk ice-softening mechanisms which are applied to the entire ice column.

Ice sheet modeling requires a choice of stress-balance equations, and improvements to SIA-only models are an active area of research. Our modeled basal sliding is modulated by a membrane stress-balance, which we believe is the leading-order change needed to improve SIA-only models. Differences between modeled and observed surface velocities are dominated by uncertain boundary processes more than by stress-balance differences, once membrane stresses are included in those balances. ("Boundary processes" include basal strength and hydrology models, in particular, but also geothermal flux inputs and calving forces.)

Ice flow integrates the influence of past climates into the enthalpy field, thereby affecting present-day distributions of ice softness and basal melt rate. A model of the paleo-climate is used to compute this influence in detail [e.g. *Huybrechts and de Wolde*, 1999]. By using a steady climate we have avoided large uncertainties in the paleo-climate. Our results suggest that identifying key boundary process parameters is of at least equal importance to choosing parameters controlling modeled paleo-climate, when matching present-day surface velocities. Nonetheless some of the modeled-versus-observed surface speed distribution differences seen in our results may follow from the actually non-steady condition of the present-day ice sheet. The GrIS is neither in balance with its present-day climate nor experiencing a steady climate, and Figure 2 suggestively shows

that many more cells have observed speeds in the 500–1500 m/a range than in the model results. This effect was robust across the model study.

Because of the critical importance of grounding lines and ice shelf buttressing for marine ice sheets, the model described in the current paper may not be, by itself, sufficient to describe the present flow condition of the Antarctic ice sheet with the same degree of agreement with observed ice velocity. By itself it is a reasonably generic model for mostly-grounded ice sheets. It can be applied in paleo-glacial circumstances in which there is no opportunity to invert extensive surface observations.

In summary, by considering only three parameters controlling ice softness and basal resistance, and by using an unprecedented 3km grid resolution uniformly over the entire ice sheet, our model achieved good agreement with newly-assembled observations of the surface velocity of the Greenland Ice Sheet. This agreement occurs even though the model is shallow and uses a steady, present-day climate. The best fit to observations occured in a run with no enhancement of ice-softness, nearly-plastic basal rheology, and high modeled basal water pressure in fast-flowing regions.

**Acknowledgments.** E. B. and C. K. received support from NASA grants NAG5-11371 and NNX09AJ38G, and I. J. and B. E. S. from NASA grants NNG06GE55G and NNX08AL98A. H. Blatter, M. Fahnestock, A. Levermann, C. Schoof, and M. Truffer all provided important insights. This work was supported by a grant of resources from the Arctic Region Supercomputing Center at the University of Alaska Fairbanks as part of the Department of Defense High Performance Computing Modernization Program.

## References

Aschwanden, A., and H. Blatter (2009), Mathematical modeling and numerical simulation of polythermal glaciers, *J. Geophys. Res.*, *114*, f01027, doi:10.1029/2008JF001028.

Bamber, J., R. Layberry, and S. Gogenini (2001), A new ice thickness and bed data set for the Greenland ice sheet 1: Measurement, data reduction, and errors, *J. Geophys. Res.*, *106 (D24)*, 33,773–33,780.

Bueler, E., and J. Brown (2009), Shallow shelf approximation as a "sliding law" in a thermodynamically coupled ice sheet model, *J. Geophys. Res.*, *114*, f03008, doi:10.1029/2008JF001179.

Burgess, E., R. Forster, J. Box, E. Mosley-Thompson, D. Bromwich, R. Bales, and L. Smith (submitted), A spatially calibrated model of annual accumulation rate on the Greenland Ice Sheet (1958–2007).

Clarke, G. K. C. (2005), Subglacial processes, *Annu. Rev. Earth Planet. Sci.*, *33*, 247–276, doi: 10.1146/annurev.earth.33.092203.122621.

Fausto, R. S., A. P. Ahlstrom, D. V. As, C. E. Boggild, and S. J. Johnsen (2009), A new present-day temperature parameterization for Greenland, *J. Glaciol.*, *55*(189), 95–105.

Hutter, K. (1983), *Theoretical Glaciology*, D. Reidel.

Huybrechts, P., and J. de Wolde (1999), The dynamic response of the Greenland and Antarctic ice sheets to multiple-century climatic warming, *J. Climate*, *12*, 2169–2188.

Jakobsson, M., R. Macnab, L. Mayer, R. Anderson, M. Edwards, J. Hatzky, H. Schenke, and P. Johnson (2008), An improved bathymetric portrayal of the Arctic Ocean: Implications for ocean modeling and geological, geophysical and oceanographic analyses, *Geophys. Res. Lett.*, *35*(7).

Joughin, I. (2002), Ice-sheet velocity mapping: a combined interferometric and speckle-tracking approach, *Ann. Glaciol.*, *34*, 195–201.

Joughin, I., B. E. Smith, I. M. Howat, and T. Scambos (submitted), Greenland flow variability from ice-sheet-wide velocity mapping.

Joughin, I., D. R. MacAyeal, and S. Tulaczyk (2004), Basal shear stress of the Ross ice streams from control method inversions, *J. Geophys. Res.*, *109*(B09405), doi:10.1029/2003JB002960.

Lliboutry, L. A., and P. Duval (1985), Various isotropic and anisotropic ices found in glaciers and polar ice caps and their corresponding rheologies, *Annales Geophys.*, *3*, 207–224.

Lüthi, M., M. Funk, A. Iken, S. Gogineni, and M. Truffer (2002), Mechanisms of fast flow in Jakobshavns Isbræ, Greenland; Part III: measurements of ice deformation, temperature and cross-borehole conductivity in boreholes to the bedrock, *J. Glaciol.*, *48*(162), 369 – 385.

MacAyeal, D. R. (1989), Large-scale ice flow over a viscous basal sediment: theory and application to ice stream B, Antarctica, *J. Geophys. Res.*, *94*(B4), 4071–4087.

Paterson, W. S. B. (1994), *The Physics of Glaciers*, 3rd ed., Pergamon.

Paterson, W. S. B., and W. F. Budd (1982), Flow parameters for ice sheet modeling, *Cold Reg. Sci. Technol.*, *6*(2), 175–177.

Schoof, C. (2006), A variational approach to ice stream flow, *J. Fluid Mech.*, *556*, 227–251.

Shapiro, N. M., and M. H. Ritzwoller (2004), Inferring surface heat flux distributions guided by a global seismic model: particular application to Antarctica, *Earth and Planetary Science Letters*, *223*, 213–224.

Tulaczyk, S., W. B. Kamb, and H. F. Engelhardt (2000), Basal mechanics of Ice Stream B, West Antarctica 2. Undrained plastic bed model, *J. Geophys. Res.*, *105*(B1), 483–494.

Weertman, J. (1964), The theory of glacier sliding, *J. Glaciol.*, *5*, 287–303.

Weis, M., R. Greve, and K. Hutter (1999), Theory of shallow ice shelves, *Continuum Mech. Thermodyn.*, *11*(1), 15–50.

E. Bueler, Dept. of Mathematics and Statistics, Chapman Hall, Univ. of Alaska, Fairbanks, Alaska, 99775-6660, USA. (elbueler@alaska.edu)

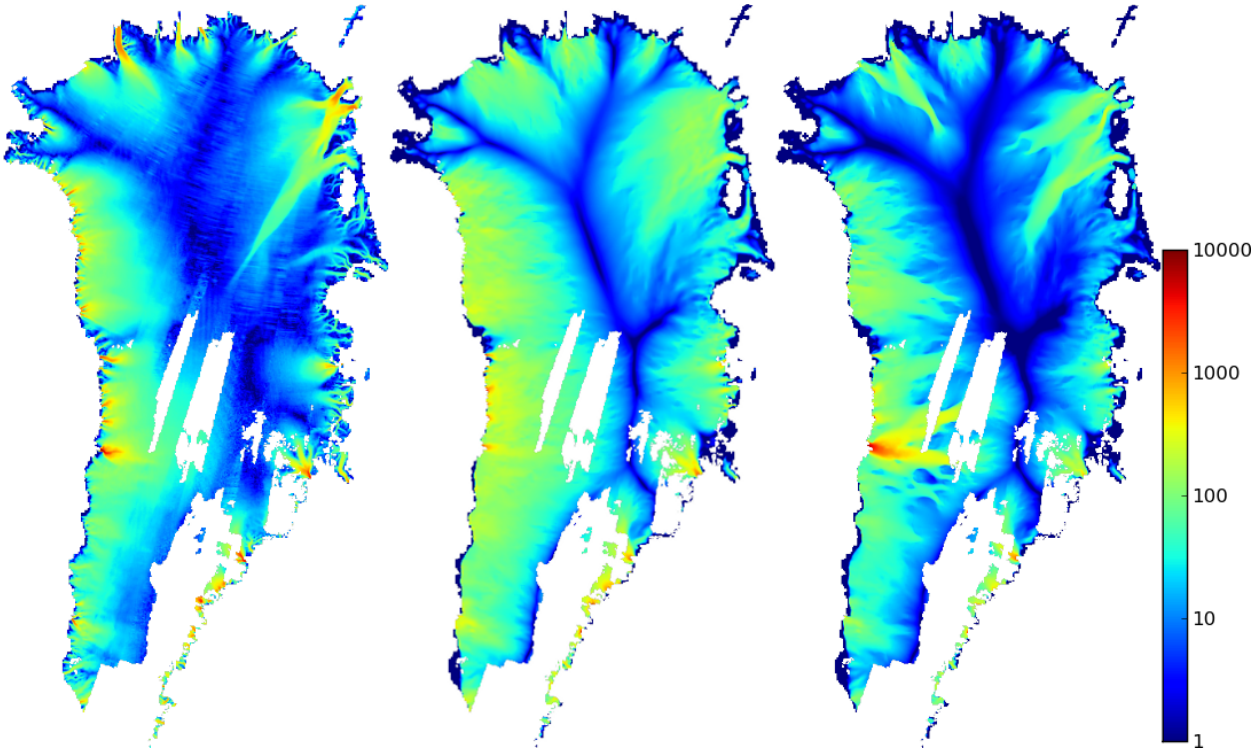


**Figure 1.** Observed (left) surface speed (m/a) versus results from two model runs: control run (middle) and best run (right), on a common logarithmic color scale. Model results are masked out where there is no observed velocity with which to compare.

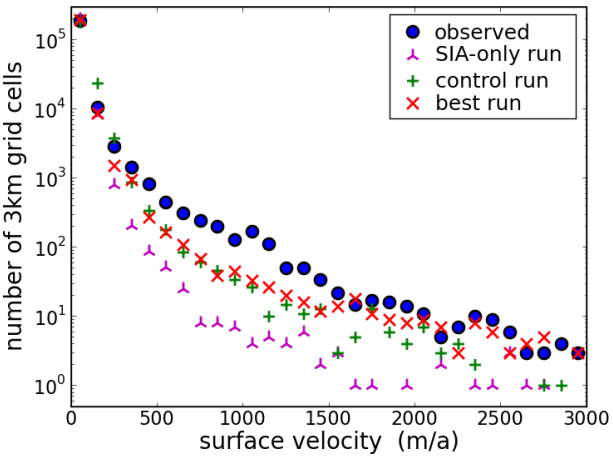


**Figure 2.** Distribution of surface speeds in observed data and in three model runs. Computed by counting the number of 3 km grid cells with speeds in each of 30 bins with boundaries $0, 100, 200, \ldots, 3000$ m/a. See text for parameter choices in model runs.